**Proceedings of ASME Turbo Expo 2015**
**GT2015**
**June 15-19, 2015, Montreal, Canada**

**GT2015-42233**

# Full Coverage Shaped Hole Film Cooling in an Accelerating Boundary Layer with High Free-Stream Turbulence

**J. E. Kingery and F.E. Ames**
Mechanical Engineering Department
University of North Dakota
Grand Forks, ND 58202

## ABSTRACT

Full coverage shaped-hole film cooling and downstream heat transfer measurements have been acquired in the accelerating flows over a large cylindrical leading edge test surface. The shaped holes had an 8° lateral expansion angled at 30° to the surface with spanwise and streamwise spacings of 3 diameters. Measurements were conducted at four blowing ratios, two Reynolds numbers and six well documented turbulence conditions. Film cooling measurements were acquired over a four to one range in blowing ratio at the lower Reynolds number and at the two lower blowing ratios for the higher Reynolds number. The film cooling measurements were acquired at a coolant to free-stream density ratio of approximately 1.04. The flows were subjected to a low turbulence condition (Tu = 0.7%), two levels of turbulence for a smaller sized grid (Tu = 3.5%, and 7.9%), one turbulence level for a larger grid (8.1%), and two levels of turbulence generated using a mock aero-combustor (Tu = 9.3% and 13.7%). Turbulence level is shown to have a significant influence in mixing away film cooling coverage progressively as the flow develops in the streamwise direction. Effectiveness levels for the aero-combustor turbulence condition are reduced to as low as 20% of low turbulence values by the furthest downstream region. The film cooling discharge is located close to the leading edge with very thin and accelerating upstream boundary layers. Film cooling data at the lower Reynolds number, show that transitional flows have significantly improved effectiveness levels compared with turbulent flows. Downstream effectiveness levels are very similar to slot film cooling data taken at the same coolant flow rates over the same cylindrical test surface. However, slots perform significantly better in the near discharge region. These data are expected to be very useful in grounding computational predictions of full coverage shaped hole film cooling with elevated turbulence levels and acceleration. IR measurements were performed for the two lowest turbulence levels to document the spanwise variation in film cooling effectiveness and heat transfer.

## INTRODUCTION

Vane internal cooling methods typically terminate with spent coolant discharge through film cooling holes or near the trailing edge. This study evaluates the most effective discharge configurations for a leading edge cooling configuration called incremental impingement [1]. The previous film cooling work in this area [2] looked at slot discharge downstream from the stagnation region of two large cylindrical leading edge test surfaces. The present research investigates the use of full coverage film cooling using shaped holes downstream from the largest of the two leading edge test surfaces.

Film cooling downstream from a leading edge is often located in regions where the local velocity is relatively low, flow is accelerating and turbulence levels are high. In these regions the coolant to discharge pressure ratio can be high relative to the dynamic pressure of the free-stream resulting in relatively high blowing ratios. Relatively high blowing ratios normally produce poor film cooling coverage due to jet penetration and mixing. The use of shaped holes can produce much better film cooling due to a reduced effective blowing ratio at the hole exit.

The present research looks at full coverage shaped-hole film cooling downstream from a cylindrical stagnation region in a highly accelerating flow. The flow is subjected to a wide range of turbulence characteristics but initially remains transitional. These data have been acquired over a wide range of blowing ratios and at two Reynolds numbers. This complex flow situation is believed to be highly relevant to film cooling situations on first vanes where similar conditions occur.

## NOMENCLATURE

b bar thickness for grid, m
$C_f$ skin friction coefficient
$C_p$ specific heat at constant pressure, kJ/kg/K
d cooling hole diameter, m
D leading edge diameter, m
h heat transfer coefficient, $W/m^2/K$
H boundary layer shape factor, $H = \delta^*/\delta_2$
k thermal conductivity, W/m/K
K acceleration parameter, $\nu/U_\infty^2 (dU_\infty/dx)$
L hole length, m
Lu energy scale, $Lu = 1.5\ u'^3/\varepsilon$, m
Lx longitudinal integral scale, m

 This work was supported under DOE grant FE0004588.

Ly normal integral scale, m
M blowing ratio, $\rho U_C/\rho_\infty U_\infty$
M mesh spacing of grid, m
P pressure, Pa
P hole pitch, m
$Re_D$ approach flow diameter Reynolds number, $\rho U_\infty D/\mu$
St Stanton number, $St = h/\rho C_P U_{EXIT}$
T temperature, °C
Tu turbulence intensity, $u'/U_\infty$
U velocity, m/s
u' streamwise rms fluctuation velocity, m/s
X streamwise distance from slot outlet, m
Y spanwise distance, m

### Greek Letter Symbols

$\delta^*$ displacement thickness, m
$\delta_2$ momentum thickness, m
$\varepsilon$ turbulent dissipation, $m^2/s^3$
$\eta$ adiabatic effectiveness, $(T_R - T_{AW}) / (T_R - T_{C,OUT})$
$\rho$ fluid density, mass per unit of volume, $kg/m^3$
$\mu$ absolute viscosity, Pa-s
$\nu$ kinematic viscosity, $m^2/s$

### Subscripts

0 turbulence condition at leading edge in absence of cylinder
AW adiabatic wall
C coolant outlet property taken at hole throat
R recovery conditions
$\infty$ taken at the free-stream

## BACKGROUND

The present film cooling paper documents film cooling effectiveness levels for a staggered array of shaped holes with strong streamwise acceleration and a range of inlet turbulence levels. Consequently, relevant literature related to this research includes discrete hole film cooling with both round and shaped holes and the influence of turbulence as well as effects of acceleration.

**Round-Hole Film Cooling.** The *Handbook of Heat Transfer Applications* [3] suggests that a number of important variables can influence discrete hole film cooling. These variables include velocity and density ratio, turbulence level and scale, displacement thickness to hole diameter, pressure gradient, curvature, injection angle and pitch to diameter ratio. L'Ecuyer and Soechting [4] surveyed the discrete hole film cooling literature including research with a wide range of density ratios and observed three regimes which they characterized using velocity ratio. They described the mass addition region at velocity ratios at or below 0.25 where film cooling effectiveness levels improved with the increasing thermal capacitance of the coolant. They described a mixing regime at velocity ratios ranging from 0.25 to 0.8 where influences of increased thermal capacitance with increasing velocity ratio opposed increased penetration with increasing momentum flux ratio. Above velocity ratios of 0.8 they described a penetration region characterized by excessive coolant penetration and increased diffusivity due to jet to free-stream interaction. L'Ecuyer and Soechting developed a correlation for discrete hole film cooling based primarily on the data of Pedersen et al. [5]. Pedersen et al. [5] studied the influence of a wide range of density ratios on film cooling. They showed that at a given blowing ratio, film cooling effectiveness levels could substantially vary with density ratio due to the variation in normal momentum with the resulting velocity ratio or momentum flux ratio. Sinha et al. [6] also investigated the influence of density ratio on effectiveness showing similar trends with Pedersen's data. Foster and Lampard [7] studied the influence of injection angle on film cooling effectiveness showing that a shallow angle significantly enhanced effectiveness levels. Pressure gradient can also have an important influence on effectiveness. Both Teekaram et al. [8] and Schmidt and Bogard [9] studied the influence of pressure gradient on film cooling. They both found enhanced laterally averaged effectiveness levels over a wide range of momentum flux ratios. The improvement was most pronounced over mass flux ratios ranging from 0.4 to 1.0. Ames [10] also found improved film cooling effectiveness levels for a single row of holes on the pressure surface of a vane with strong favorable acceleration compared with the suction surface where the local pressure was mildly adverse for his low turbulence case. Ito et al. [11] investigated the influence of curvature on laterally averaged effectiveness. They found convex curvature resulted in significantly improved effectiveness levels while concave curvature caused a significant deterioration up to the penetration regime. Schwartz et al. [12] looked at curvature effects on film cooling in a zero-pressure gradient test section and found similar results. Film cooling coverage can also be improved using two staggered rows of holes. Jabari and Goldstein [13] compared two staggered rows of holes with a single row at the same blowing ratio (0.5) and density ratio (0.84) and found improved film cooling effectiveness over a single row of holes superposed. Ames [10] looked at one and two rows of holes on the pressure surface of a vane and at velocity ratios of 1.0 and 1.5 found significantly improved effectiveness levels compared with one row of holes superposed. A double staggered row causes more flow blockage with the free stream than a single row and this blockage is believed to result in the enhanced laydown of the jets. Liess [14] investigated the influence of displacement thickness to diameter ratio on a zero velocity gradient flow at blowing ratios ranging from 0.31 to 0.43. He found laterally averaged effectiveness began to deteriorate at displacement thickness to diameter ratios greater than about 0.1 which causes local blowing ratios which are effectively higher. Burd et al. [15] studied the influence of hole length to diameter ratio (L/d) and concluded that short holes produced "jetting" further into the free-stream than longer holes.

**Effects of Turbulence on Discrete Hole Film Cooling.** Addressing the influence of turbulence on film cooling may be the most important variable in modern film cooling designs. Kadotani and Goldstein [16, 17] investigated the influence of turbulence characteristics (turbulence level, 0.3% to 20.6% and scale, Ly/d = 0.06 to 0.33) on film cooling. They found enhanced free-stream jet mixing with both increased turbulence level and increased scale. Simon [18] considered the influence of free-stream turbulence on slot film cooling. He developed an analytical model grounded in the work of several investigators which included a potential core region and a fully developed region where film cooling dissipation was related to the growth of the jet boundary layer. Bons et al. [19] investigated the influence of turbulence level (0.9% to 17%) on a single row of holes (P/d = 3.0) with a 35° angle with the surface. They generally found increased dissipation of centerline film cooling with increased turbulence level and downstream distance at moderate velocity ratios. They noted complete spanwise mix out by X/d = 10 at their highest turbulence level. Kohli and Bogard [20] studied discrete hole film cooling at turbulence levels of 0.5% and 20%. They initially found the mixing between the free-stream and jet was largely due to jet to free-stream shear layer structures while at high turbulence, flow field turbulence structures quickly dominated the mixing process. Ames [10, 21] investigated vane film cooling at low

(Tu = 0.9%) and high (Tu = 12.4%, Lu/d = 25) turbulence levels for single and double row film cooling. On the pressure surface of the vane where turbulence levels were highest, he noted the incremental dissipation of film cooling effectiveness levels by nearly 60% at an X/d of 68. Mayhew et al. [22] used liquid crystal thermography to visualize the rapid spreading and dissipation of film cooling at a blowing ratio of 0.5 due to a turbulence intensity of 10%. However, similar to other investigators their data indicated an improved level of film cooling in the near-hole region at higher blowing ratios (1.0 and 1.5) due to the high turbulence level.

**Shaped-Hole Film Cooling.** Bunker [23] conducted a review of shaped hole film cooling indicating that work in this area was initiated more than 40 years ago. He suggested that the use of shaped holes on turbine airfoils was perhaps the single primary advancement seen in film cooling in the last 30 years. He cited the work of Thole et al. [24] and Haven et al. [25] to observe that laterally and forward expanded hole shapes can lead to lower film effectiveness than laterally expanded holes due to excessive diffusion of the jet and the resulting interactions with the free-stream flow. He indicated that the most significant drawback of shaped holes was related to the aerodynamic penalty due to the injection of low momentum fluid into a high speed flow. Recently, Schroeder and Thole [26] reviewed the literature of shaped holes noting a wide range of geometries. They offered the gas turbine community a "baseline" shaped hole with a 30° incline, a 7° degree lateral diffusion and a 7° layback. Generally, shaped holes appear to suffer from similar issues as round holes such as jet penetration with higher blowing ratios. However, shaped holes can be used at much higher blowing ratios before these effects become a problem. However, one effect that appears to influence shaped holes even more than round holes is free-stream turbulence. Saumweber et al. [27] and Saumweber and Schultz [28] studied the influence of free-stream turbulence on round and shaped holes. They show how a separation bubble inside a 14° expanded hole results with a double peak in the film cooling distribution. They concluded that the benefit of shaped holes over round holes is significantly overestimated when based on low turbulence comparisons. They noted that while turbulence can lead to improved film cooling performance in round holes when blowing ratios begin to reach the penetration regime, turbulence generally makes the dissipation of film cooling more rapid for shaped holes.

**Considerations.** The present paper investigates a staggered row of shaped holes in a highly accelerating and transitioning flow field typical of gas turbine vane pressure and near suction surfaces. The lateral expansion of the film cooling holes was set at 8° to avoid separation inside the holes and provide nearly optimum coverage for the 2 row staggered array. The boundary layer approaching the film cooling is very thin, typical of the near suction surface or pressure surface where acceleration is high. The wall thickness is double the hole diameter which is typical of most vane cooling designs. This film cooling database was generated across six turbulence conditions with intensities ranging from 0.6% to 13% and at four blowing ratios ranging from 0.55 to 1.9. The data were acquired over a 2 to 1 range in Reynolds number to provide information about how the state of the boundary layer influences film cooling levels. This database includes downstream heat transfer measurements to show the influence of injection as well as the state of the boundary layer. This database is expected to be highly useful in the development of design tools for the prediction of film cooling for gas turbine application.

## EXPERIMENTAL APPROACH

Adiabatic film cooling and heat transfer measurements were acquired downstream of the shaped hole insert over the large cylindrical leading edge test surface. The leading edge test surface was mounted at the midline of a rectangular spool and placed downstream from the large scale low speed cascade wind tunnel facility shown in Figure 1. As pictured schematically the wind tunnel shows the low turbulence condition but it can be configured to integrate the five higher turbulence conditions used in the present study. The shaped hole insert was integrated into the film cooling and heat transfer test surface which previously was used for a slot film cooling study [2]. The test surface profile produces a strong initial acceleration at and directly downstream of the film cooling injection. Both adiabatic temperature and heat transfer measurements were acquired over the test surface for the full range of conditions. Additionally, full surface film cooling and heat transfer data were acquired using an IR camera at the two lowest turbulence levels to compare with the span averaged thermocouple measurements.

**Low Speed Wind Tunnel.** The wind tunnel used in the acquisition of these film cooling and heat transfer measurements is shown schematically in Figure 1. The initial tunnel flow is entrained into the blower through a large filter box holding 8-1 $m^3/s$ high efficiency industrial pocket filters. The blower is powered by a 45 kW motor controlled with a variable frequency drive. The blower is capable of delivering 6.6 $m^3/s$ of flow at a static pressure rise of 5000 Pa. The blower discharges into a two-stage multi-vane diffuser designed to recover pressure from the blower and to spread out the flow into a heat exchanger. The heat exchanger system includes a recirculation system consisting of a pump and a 0.4 $m^3$ tank. The system operates continuously and is controlled to keep the tunnel air temperature constant during film cooling and heat transfer tests.

The heat exchanger system can produce a steady cross-passage temperature stratification at the highest Reynolds number. This stratification is largely mixed away when using the high turbulence generators but can still be present in the flow at specific conditions. Generally, heat transfer and film cooling measurements have always included an adiabatic measurement before the cooled film cooling air or heated wall measurements. Consequently, this stratification has largely been either mixed out and/or subtracted out. However, this problem can cause increased uncertainty in the adiabatic film cooling measurements. A cross passage mixer and flow straightener has been installed downstream from the heat exchanger in the spacer. The flow from the flow straightener is discharged into the screen box which consists of four nylon window screen and is designed to remove lateral velocity variations. The screen box flow discharges into a 3.6 to one area ratio contraction nozzle which in turn discharges into the test section containing the leading edge test surface. This baseline configuration is used to generate the low turbulence (LT) condition.

**Turbulence Generation.** Five elevated turbulence conditions were generated and used in the present film cooling and heat transfer tests. These conditions along with the low turbulence condition are tabulated in Table 1. These values are based on previous measurements in the facility, which have characterized the turbulence for the various turbulence generators [29-31]. The turbulence characteristics provided in Table 1 include turbulence intensity (Tu), the longitudinal integral scale (Lx), the energy scale (Lu), and the turbulent dissipation ($\varepsilon$) for the given velocity ($U_{AVE}$). These turbulence characteristics were acquired using hot wire anemometry and are based on the composite of several locations and in some cases more than one measurement. All the measurements are based on the composite of the velocity time records used to determine the one dimensional energy spectrum of u' for consistency. The turbulence intensity (Tu) is determined from the unbiased estimate of u' divided by the mean velocity. The longitudinal integral scale (Lx) is

 

determined from the autocorrelation time scale times the local mean velocity assuming that Taylor's hypothesis is reasonably valid. The autocorrelation in time is determined from an inverse FFT of the averaged energy spectrum of u'. The turbulent dissipation (ε) was determined from the inertial subrange of the energy spectrum. Subsequently, the energy scale (Lu) was determined from this dissipation rate and the local value of u'. The measurements can be interpreted as values which would occur at the streamwise location of the stagnation point in the absence of the leading edge test surface.

Film cooling experiences a wide range of turbulence levels from the low velocity regions of the pressure surface through the high velocity regions of the furthest downstream regions of injection on the suction surface. The six turbulence conditions were generated to investigate the influence of a range of turbulence appropriate to the conditions present on a typical cooled turbine airfoil. The present conditions include aero-combustor (AC) turbulence (13%) with an energy scale of around 7 cm. The aero-combustor (AC) condition was generated by replacing the 3.6 to 1 contraction nozzle with the simulated combustor turbulence generator. A second level of aero-combustor turbulence (Tu = 9%, Lu = 9 cm) is generated by placing a 91.4 cm long rectangular spool between the aero-combustor and the film cooling test section. Three elevated turbulence conditions were generated with grids. The larger grid (b = 1.27 cm, M = 6.35 cm) turbulence (GR) was generated by placing the larger grid in the decay spool ten mesh lengths upstream of the leading edge plane of the test surface. The grid configurations used the low turbulence nozzle with the rectangular spool upstream of the test section. Two levels of turbulence were generated with the smaller grid (b = 0.635 cm, M = 3.175 cm). The near position (SG1) was 10 mesh lengths upstream of the leading edge plane and the far position (SG2) was placed 32 mesh lengths upstream. Both grids produced turbulence levels of around 8% when placed 10 mesh lengths upstream with energy scales of about 3.4 cm and 1.9 cm. The small grid in the far position generated a turbulence level of 3.5% with an energy scale of 3.0 cm. The low turbulence condition generated a turbulence level of 0.7%.

**Shaped Hole Geometry and Film Cooling Plenums.** The shaped hole film cooling insert was designed to fit into the leading edge of the larger test surface used for slot and shaped hole film cooling measurements. The plenum is shown schematically as a wire frame in Figure 2. The leading edge insert which holds the film cooling plenum and the shaped hole array is designed to fit centered on the cylindrical leading edge of the test surface. The leading edge radius is constant over the first +/- 30° of the surface and then increases monotonically to produce a smooth velocity and acceleration profile. The film cooling flow enters the insert through a 5.08 cm schedule 40 PVC pipe. The flow from the pipe discharges into the pie shaped chamber opposite to the inlet of the simulated double wall cooling section. The double wall cooling section includes an inlet, three staggered rows of 1.68 cm diameter pins and later two more rows of pins. The pins are spaced at 1.625 diameters in the cross passage direction and 1.074 diameters in the streamwise direction. The rows of pins are designed to simulate the turbulence and unsteadiness of a high solidity double wall cooling channel. Downstream from the last row of pins, the flow moves into a 1.27 cm high constant height duct before being directed into the two staggered row, full coverage shaped-hole film cooling array.

The shaped holes have an 8° lateral expansion slanted at 30° to the surface as shown in Figure 3. The 0.559 cm holes have a spanwise pitch of 3 diameters and streamwise spacing of 3 diameters along the surface. The array has been designed to provide full coverage film cooling. The lateral expansion was designed to be conservative to reduce the potential for separation inside the holes. The top wall has a thickness of 1.68 cm providing an L/D of 4. The lateral expansion begins at the point the hole is entirely surrounded by material leaving 1.75 cm of distance for lateral expansion. The centerline of the hole emerges with a width of approximately 1.05 cm or an area of roughly 2.1 times the round hole. When the top of the hole emerges, the area ratio is about 1.8 and the spanwise width to hole diameter is 1.63. The minimum area in the hole is used to determine the blowing ratio.

**Film Cooling and Heat Transfer Surface.** The shaped-hole film cooling plenum is removable and attaches directly to the film cooling and heat transfer test surface as shown in Figures 4 and 5. The bracket which holds the plenum is fastened to the surface and includes two static pressure taps and three surface thermocouples, which are directly downstream from the shaped-hole film cooling array. Downstream from the pressure taps and surface thermocouples the bracket is designed to accept the constant heat flux foil bus bar. The bracket also attaches to the epoxy board which holds the downstream surface thermocouples and produces a smooth covering for the isocyanurate foam test surface. The epoxy board holds 60 downstream surface thermocouples positioned at 20 streamwise locations, each with 3 spanwise positions including midspan and +/- 5.08 cm. The initial spacing is much more concentrated compared with the downstream spacing as outlined in [2]. The constant heat flux heater is comprised of a 0.023 mm Inconel foil which is adhered to a 0.05 mm thick Kapton surface. The Kapton surface is backed with thin layer of high temperature pressure sensitive acrylic adhesive which adheres the foil to the epoxy board. The foil has a 0.635 cm wide, 0.5 mm thick copper buss bar on each end to allow the application of a high heat flux during heat transfer measurements. The foil is not heated during film cooling data acquisition. The isocyanurate foam sheets used to form the heat transfer test surface were fabricated using a precision router jig of the profile.

**Test Surface Shape, Velocity Profile, and Acceleration.** The half profile of the heat transfer test surface is shown schematically in Figure 6 along with the top of the test section. The test surface was designed to accommodate the 0.4064 m diameter leading edge over +/- 30°. The profile then transitions smoothly from the high acceleration of the leading edge to an exit velocity about double the approach velocity. The predicted velocity distribution is presented in Figure 7 and is based on a 2D Fluent [32] analysis. The Fluent model consisted of approximately 7600 quadrilateral cells and included a boundary layer mesh. The computation used an implicit pressure based solver along with the Spalart-Allmaras [33] one equation eddy diffusivity transport model for turbulence closure. The velocity distribution shown in Figure 7 is determined from the surface local isentropic Mach number based on the predicted pressure distribution. The velocity determined from the static pressure tap on the bracket is typically within 2% of the predicted velocity at that position for the taped hole condition. The initial velocity increase at the leading edge is nearly linear before the acceleration rate begins to slow just downstream from the exit of the film cooling array. Here, the velocity is plotted in terms of the distance from the exit of the downstream row of film cooling holes. The acceleration parameter K ($K = \nu/U^2\, dU/dx$) was determined for the 250,000 Reynolds number case and was found to stay above the relaminarization criteria (K > 3E-6) for the first 11 hole diameters downstream from the coolant discharge. This level of acceleration indicates that the flow on the surface could remain laminar or transitional for a significant portion of the test surface. The K value is half the 250,000 Reynolds number value for the 500,000 Reynolds number case.

**Upstream Boundary Layers.** Hot wire traverses were conducted on the large diameter leading edge test surface to characterize the

upstream boundary layer. The velocity distribution of the upstream boundary layer can have a significant influence on film cooling effectiveness. The profiles were surveyed 9.61 cm downstream from the stagnation line using a single hotwire powered with a TSI IFA 300 constant temperature anemometry bridge. The momentum thickness ($\delta_2$) averaged 0.094 mm with a shape factor (H) of 2.2 at the 250,000 Reynolds number. The momentum thickness averaged 0.074 mm for the 500,000 Reynolds number condition with a comparable shape factor. The displacement thickness averages about 3.7% and 2.9% of the hole diameter at the lower and higher Reynolds number. The shape factor is consistent with a 2D leading edge stagnation region. The very full and thin upstream boundary layer provides a nearly ideal situation for good film cooling [14].

**Infrared Camera Measurements.** Full field infrared thermography measurements were acquired at the low (LT) and small grid far (SG2) turbulence conditions. These measurements were made to assess the spanwise variation of film cooling effectiveness and heat transfer at these conditions. These turbulence conditions were expected to have the highest spanwise variation in film cooling effectiveness and surface heat transfer. Higher levels of turbulence are known to cause significant spanwise mixing of film cooling [10].

The heat transfer surface was painted flat black in preparation for the infrared (IR) measurements. Subsequently, dots of low IR emissivity metallic paint were applied every 5.08 cm in the streamwise direction at midspan and +/- 6.35 cm to provide a grid of points for location identification. The temperatures for the entire IR image were corrected based on a calibration between the thermocouple temperatures and the local IR temperatures. This correction was only made in the streamwise direction to avoid correcting out the spanwise variation in the film cooling effectiveness or heat transfer measurements.

**Film Cooling Supply and Measurements System.** The film cooling supply was generated using a window air conditioning unit. The inlet of A/C unit evaporator was ducted directly to a small pressure blower controlled with a variable frequency drive. The exit of the evaporator was ducted to a thermal capacitance system which in turn was ducted into a sharp edged orifice tube for flow measurement. Downstream of the orifice the air was ducted to the PVC tube connected to the film cooling plenum. All the components downstream from the A/C unit evaporator were insulated.

**Uncertainty Estimates.** Uncertainties in the reported film cooling effectiveness and surface Stanton number were determined with the root sum square method described by Moffat [34]. In this paper effectiveness levels and surface Stanton number are based on the spanwise average of three thermocouples. The standard deviation film cooling effectiveness in the spanwise direction can be estimated using the IR images. Based on this assessment at the low turbulence level the uncertainty in the reported effectiveness has been estimated to be +/- 0.053 in the near hole region and +/- 0.039 at around 40 diameters downstream. Comparisons of spanwise variation in effectiveness between the low turbulence condition and the small grid far condition suggests the spanwise variation decreases as turbulence level increases which will cause the uncertainty of the film cooling measurements to decrease. Consequently, the uncertainty at the higher turbulence levels was estimated to be +/- 0.035 in the near field where effectiveness levels are high and +/- 0.025 in the far field where effectiveness levels are lower. The uncertainty in the downstream Stanton number was estimated to be approximately +/- 0.0001 or about +/-5%. The uncertainty in the near field Stanton number was estimated to be as high as +/- 0.0003. This large near field uncertainty in Stanton number is due to the unheated starting length effect of the foil and the discrete hole injection of the film cooling array. The resulting uncertainty was estimated to be as high as +/- 8% of the local near field value. The uncertainty in the reported turbulence intensity is believed to be +/- 3% of the reported values. The uncertainty in the reported turbulent scales is estimated to be about +/- 13%. These uncertainties are provided at 95% confidence limits.

## EXPERIMENTAL RESULTS

This shaped hole film cooling experiment investigated film cooling effectiveness and heat transfer distributions in a highly accelerating flow field subjected to a range of engine relevant turbulence levels. The measurements were acquired at four blowing ratios and two Reynolds numbers. The data were acquired at six separate turbulence conditions. Infrared temperature measurements were acquired to evaluate the spanwise variation of film cooling and heat transfer at the two lowest turbulence conditions. The staggered double row of 8° lateral expansion shaped holes is believed to be a film cooling design relevant to the gas turbine community.

**Blowing Ratio Comparisons.** A comparison between film cooling effectiveness distributions for the four blowing ratios at the low turbulence condition is presented for the 250,000 approach flow Reynolds number in Figure 8. The M = 0.54 conditions shows a good level of effectiveness and the M = 0.97 condition shows a significant incremental increase above the lower blowing ratio case. However, at M = 1.34 the incremental increase in film cooling effectiveness is much more modest indicating the normal momentum is moving into the high mixed flow regime toward the penetration regime. The area ratio of the hole at a point perpendicular to the centerline breakout point is 2.11 giving an effective velocity ratio of about 0.61 at this blowing ratio. By an M = 1.89 the effectiveness distribution is now lower than the blowing ratio half its value indicating poor film cooling distribution due to excessive penetration. A similar comparison is shown for the small grid far turbulence condition presented in Figure 9. This condition produces a local turbulence level of about 3.2% at the discharge location which is reasonably consistent with turbulence level on the suction surface of a vane where the velocity is significantly higher than the inlet value. The effectiveness distributions show significant decay due to the turbulence indicating only about half the low turbulence effectiveness levels at the end of the plate for the two lowest blowing ratios. However, the M=1.35 condition now shows a more significant increase over the M = 0.97 blowing ratio than the low turbulence case. Also, the highest blowing ratio now has an effectiveness level consistent with the M = 1.35 case. The grid turbulence case is presented in Figure 10. This turbulence condition produces a turbulence level of about 7.4% at injection. This intensity would be consistent with a turbulence level encountered by film cooling at a medium velocity along the vane surface such as near suction side or far downstream on the pressure surface. The effectiveness distributions are now well ordered on the blowing ratio indicating the importance of mass addition at higher turbulence levels. However, generally the level of decay is much more rapid than the two lower turbulence levels. The adiabatic effectiveness distributions for the aero-combustor turbulence are presented in Figure 11. The decay of the effectiveness level is now extremely rapid due to the turbulent mixing. The effectiveness levels clearly order almost proportionately on the blowing ratio downstream on the surface. This suggests that the film cooling is now well mixed across the boundary layer which is clearly growing rapidly due to the very high level of turbulence. This turbulence level is consistent with regions along the pressure surface of a vane.

**Turbulence Condition Comparisons.** A comparison of film cooling distributions at a blowing ratio of 0.54 at the six turbulence conditions is presented in Figure 12. The large influence of turbulence is evident in the downstream region. However, the impact of turbulent mixing appears to be immediate. The effectiveness levels order on turbulence intensity. Some impact showing increased mixing with larger scale can be noted based on the comparison between the larger and smaller grid. A comparison of effectiveness levels for the 0.97 blowing ratio is presented in Figure 13 for the six turbulence conditions with qualitatively similar results to the lower blowing ratio. Clearly, the local turbulence level at injection is a vital parameter in the development of any robust and reliable cooling design which involves film cooling.

**Reynolds Number Comparisons.** The impact of the Reynolds number in the present data is shown with comparisons between the lower and higher Reynolds number case in Figures 14 and 15. Distributions at the lower and higher Reynolds number are compared at four turbulence conditions in Figure 14 for a blowing ratio of 0.54. Over the first 75 hole diameters the lower Reynolds number cases all show superior film cooling effectiveness. This improvement is tied to the transitional state of the boundary layer as will be shown later. A comparison of the lower and higher Reynolds number is shown at the 0.96 blowing ratio for the four turbulence cases in Figure 15 with qualitatively similar results. However, at this higher blowing ratio the difference in results is much less significant. Previous studies have often tripped the boundary layer to show the effect of film cooling for turbulent flow. However, considering the use of shaped holes is typically in regions of vanes where the blowing ratio can be high and consequently the velocity is significantly below the exit velocity. These regions typically have very high acceleration, consistent with transitional flow, which is a variable which must be considered in a range of applications.

**Shaped Hole versus Slot Comparisons.** Slot film cooling is often considered the ideal [23] approach to film cooling delivery. In the present case data have been acquired for both a two-dimensional slot and the present shaped hole array over the same test surface. Also, the data were run at the same coolant flow rates for the same turbulence conditions and Reynolds numbers. The first comparison between the slot film cooling and the current shaped holes is shown in Figure 16 for a shaped hole array blowing ratio of 0.54. This corresponds to a blowing ratio of 0.42 for the slot used in reference [2]. The data are compared for the low turbulence (LT), small grid far (SG2) and the large grid (GR) turbulence conditions. The slot significantly out performs the shaped holes over the first 40 cm of the test surface in all three cases. The second comparison between the slot and shaped holes is presented in Figure 17 for a shaped hole blowing ratio of 0.97. The slot performance is still significantly higher in the near hole region. However, now the difference is much less that in the lower blowing ratio. Also, the downstream effectiveness level comparison is very consistent supporting the concept of a film layer mixed across the growing boundary layer.

**Stanton Number distributions.** Stanton number distributions provide both an indication of the level of disruption caused by the film cooling discharge as well the state of the boundary layer. The velocity distribution shown in Figure 7 suggests a boundary layer environment which is very stabilizing in terms of the onset and path to transition. Figure 18 presents Stanton number distributions taken downstream of the shaped hole film cooling array for the case of no blowing at an approach flow Reynolds number of 250,000. In this case the holes on the shaped hole array are taped to reduce the disruption of the holes on the surface. The stabilizing environment produces predominately laminar flow for the low turbulence condition and transitional flow for the other conditions, at least for the majority of the test section. The changes to the onset and path of transition are apparent for the small grid far (SG2), the other grid conditions and aero-combustor with spool (SG1, GR, and ACS) and the aero-combustor (AC) turbulence conditions. A simple model of film cooling suggests that film cooling effectiveness dissipates with the growth of the boundary layer. Obviously, if boundary layers can be kept thin and laminar then film cooling levels can be substantially improved. The influence of blowing on Stanton number and the state of the boundary layer can be determined from the distributions for a blowing ratio of 0.97 presented in Figure 19. The Stanton number data show the effect of blowing with earlier transition which moves upstream with increasing turbulence level. The 0.97 blowing ratio appeared to be less disruptive to heat transfer than the 0.54 blowing ratio. The highest Reynolds number case is presented at a blowing ratio of 0.54 in Figure 20 showing much earlier transition compared with Figure 19. Transition appears to begin by an X/d = 15 and finish by an X/d of 20. This early transition explains the improved film cooling for the lower over the higher Reynolds number cases as shown by the comparisons in Figures 14 and 15.

**Full Surface Data with Thermocouple Comparisons.** Full surface film cooling and heat transfer data were acquired for the low turbulence (LT) and small grid far (SG2) conditions. These data sets were acquired to report spanwise variations in film cooling and heat transfer and to enable the assessment of the uncertainty in the results due to this spanwise variation. Adiabatic film cooling effectiveness levels are reported in Figure 21 for the low turbulence condition at a blowing ratio of 0.54 at an approach flow Reynolds number of 250,000. The distributions cover X/d's ranging from about 2.5 to 42 in the streamwise direction and about +/- 14 diameters in the spanwise direction. The blue dots represent thermally reflective dots painted on the centerline and at +/- 6.35 cm and spaced 5.08 cm in the streamwise direction. The IR images were processed by fitting the film cooling and adiabatic thermal image to the local surface thermocouple measurements and subtracting the images. The coolant out temperature was based on the measured values at the exit of three select holes. The data in Figure 21 show some spanwise variations. The calculated standard deviation over the central +/- 12 hole diameters was determined to be +/- 0.036 in the near field and +/- 0.025 in the downstream region. Based on the three thermocouple measurements in the spanwise direction, the uncertainty in the film cooling effectiveness in the spanwise direction is as high as +/- 0.042 and as low as +/- 0.03. The major variability downstream appears to be caused by the grouping of jets. This type of grouping has been reported previously by Martini and Schultz [35] who investigated film cooling through circular wall jets discharging from a trailing edge cutback. They found this grouping produced regions of high as well as relatively poor film coverage. They also observed that the jets could regroup into different patterns. However, the level of spanwise variation in this full coverage array is not large.

A second visualization of film cooling effectiveness is presented in Figure 22 for the low turbulence at a blowing ratio of 0.97 at a Reynolds number of 250,000. This case exhibits about 10% less variation than the visualization shown in Figure 21. However, in the present case the variation is greater in the downstream region rather than the upstream region. This visualization exhibits a jet grouping of the film cooling similar to Figure 21. The third and final film cooling visualization is presented in Figure 23 for the small grid far (SG2) condition at a blowing ratio of 0.97 for a Reynolds number of 250,000. In this figure the patterns of film cooling effectiveness look similar to Figure 22. However, the enhanced spanwise mixing is

apparent and the streaks of grouped jets wash out more quickly. Here the peak variation is about 12% less than in Figure 22.

The spanwise variation in film cooling effectiveness increases the uncertainty of results based on the spanwise average of the three thermocouple rows. These rows are located on the centerline and at +/- 5.08 cm. A comparison between film cooling values determined from the average of the thermocouples and the average of the IR image are presented in Figure 24. This comparison suggests a good agreement between the sparse array of thermocouples and the IR image. A plot showing the effectiveness levels determined from the three thermocouples compared with local effectiveness levels as a function of spanwise position is provided in Figure 25. This figure presents the comparison for the low turbulence condition at the 0.97 blowing ratio for the 250,000 Reynolds number. The spanwise variation in local film cooling effectiveness provides a means to develop a well resolved spanwise standard deviation for the image which has been used in the uncertainty estimate. The plot of the 0.97 blowing ratio at the small grid far (SG2) condition for the 250,000 Reynolds number is presented in Figure 26 and provides another indication of the influence of the turbulence on spanwise mixing.

Noting that the adiabatic effectiveness has noticeable spanwise variations, the Stanton number distribution can also be expected to exhibit similar qualities. The full surface image of Stanton number is presented in Figure 27 for the low turbulence condition at a blowing ratio of 0.97 and a Reynolds number of 250,000. The patterns of heat transfer variation are much more visible and structured than the variation in film cooling. The spacing of the heat transfer variations are consistent with pitch of the holes. Although the patterns are clearly present they also exhibit a reasonable level of uniformity across the span and in the streamwise direction. The data show a decreasing Stanton number followed by an increase starting at an X/d of 30 due to transition. This pattern is consistent with the Stanton number distribution of Figure 19 for the low turbulence condition.

## SUMMARY AND CONCLUSIONS

Adiabatic effectiveness and Stanton number distributions have been acquired downstream from a full coverage array of 8° laterally diffusing shaped holes integrated into a leading edge test surface. The film cooling is discharged into a highly accelerating flow and is subjected to six well documented turbulence conditions (0.7% to 13.7%). The data are acquired over four distinct blowing ratios (0.54, 0.97, 1.35, and 1.9) and at two approach flow Reynolds numbers ($Re_D$ = 250,000 and 500,000). The present shaped hole database has been acquired at the same conditions as an earlier film cooling study for a 30° slot [2].

At the lower blowing ratios (0.54 and 0.97) and turbulence levels (0.7% and 3.5%) the full coverage shaped hole array produces high and significantly increasing levels of film cooling effectiveness. At higher blowing ratios (1.35 and 1.9) the increase in effectiveness level is incremental and even negative. However, at higher turbulence levels the decay of film cooling coverage is rapid and film cooling effectiveness levels scale very closely with blowing ratio.

Comparisons between lower and higher Reynolds number cases show a significant advantage at the lower Reynolds number for lower blowing ratios. This advantage is due to the transitional nature of the boundary developing at the lower Reynolds number.

Comparisons between slot film cooling and full coverage shaped hole film cooling show a notable advantage with the slot film cooling that disappears by the end of the test surface. This downstream equivalence between the slot and shaped hole film cooling at similar coolant flow rates supports the heat sink concept where the coolant is mixed out across the downstream turbulent boundary layer.

Aero-combustor turbulence length scale to film cooling hole diameter (Lu/d ≅ 12.5) is consistent with a medium sized gas turbine. Generally, increasing length scale causes a moderate increase in film cooling dissipation at similar inlet turbulence levels.

Full surface visualizations of film cooling provide evidence of some spanwise grouping of coolant jets. However, the spanwise variation in effectiveness remains a secondary result for this full coverage film cooling array.

The streamwise decay of film cooling due to turbulence conditions has been shown to be a dominating influence on film cooling. The data clearly show that turbulence condition at discharge is a critical variable which must be considered in the application of film cooling coverage.

## ACKNOLEGEMENTS

This work was sponsored by a grant from the National Energy Technology Laboratory of the US Department of Energy and the University of North Dakota. The views expressed in the article are those of the authors and do not reflect the official policy or position of the Department of Energy or U.S. Government.

## REFERENCES

[1] Busche, M.L., Moualeu, L.P., Chowdhury, N., Tang, C., Ames, F.E., 2013,"Heat Transfer and Pressure Drop Measurements in High Solidity Pin Fin Cooling Arrays with Incremental Replenishment," *J. Turbomach*, v. 135, 041011-1-9.

[2] Busche, M.L., Kingery, J.E., and Ames, F.E., 2014, "Slot film cooling in an accelerating boundary layer with high free-stream turbulence," ASME Paper No. GT2014-25360.

[3] Rohsenow, Hartnett, and Ganic, 1985, *Handbook of Heat Transfer Applications*, 2nd ed., McGraw-Hill, New York.

[4] L'Ecuyer, M. R., and Soechting, F. O., 1985, "A model for correlating flat plate film cooling effectiveness for rows of round holes," *Heat Transfer and Cooling in Gas Turbines: AGARD Conference Proceedings No. 390.*

[5] Pedersen, D. R., Eckert, E. R. G., and Goldstein, R. J., 1977, "Film cooling with large density differences between the mainstream and the secondary fluid measured by the heat-mass transfer analogy," *J. Heat Transfer*, Vol. 99, p. 620.

[6] Sinha, A.K., Bogard, D.G., and Crawford, M.E., 1990, "Film Cooling Effectiveness Downstream of a Single Row of Holes with Variable Density Ratio," ASME Paper No. 90-GT-43.

[7] Foster, N.W., and Lampard, D., 1980, "The Flow and Film Cooling Effectiveness Following Injection through a Row of Holes," *J. Eng. Gas Turbines Power*,, v. 102, pp. 584-588.

[8] Teekaram, A. J. H,, Forth, C. J. P., and Jones, T. V., 1991, "Film cooling in the presence of mainstream pressure gradients," *J. Turbomach.*, v. 113, p. 484.

[9] Schmidt, D. L., and Bogard, D. G., 1995, "Pressure gradient effects on film cooling," ASME Paper No. 95-GT-18.

[10] Ames, F.E., 1998, "Aspects of Vane Film Cooling with High Turbulence: Part II - Adiabatic Effectiveness," *J. Turbomach*, **v.** 120, pg. 777-784.

[11] Ito, S., Goldstein, R.J., and Eckert, E.R.G., 1978, "Film cooling of a Gas Turbine Blade," *J. Eng. Gas Turbines Power*, v. 100, pg. 476-481.

[12] Schwarz, S.G. and Goldstein, R.J., 1990, "The influence of curvature on film cooling performance," ASME Paper No. 90-GT-10.

[13] Jabbari, M.Y., and Goldstein, R.J., 1978, "Adiabatic Wall Temperature and Heat Transfer downstream of Injection Through Two Rows of Holes," J. Eng. Gas Turbines Power, v. 100, pp. 303-307.

 

[14] Liess, C., 1975, "Experimental investigation of film cooling with ejection from a row of holes for the application to gas turbine blades," *J. Eng. Gas Turbines Power*, v. 97., p. 21-27.
[15] Burd, S.W, Kaszeta, R.W, and Simon, T.W., 1998, "Measurements in Film Cooling Flows: Hole L/D and Turbulence Intensity Effects," *J. Turbomach*, v. 120, pp. 791-798.
[16] Kadotani, K., and Goldstein, R.J., 1979, "On the Nature of Jets Entering a Turbulent Flow Part A—Jet-Mainstream Interaction," *J. Eng. Gas Turbines Power*, v. 101, pp. 459-465.
[17] Kadotani, K., and Goldstein, R.J., 1979, "On the Nature of Jets Entering a Turbulent Flow Part B—Film Cooling Performance," *J. Eng. Gas Turbines Power*, v. 101, pp. 466-470.
[18] Simon, F.F, "Jet Model for Slot Film Cooling with Effect of Free-Stream and Coolant Turbulence", *NASA Technical Paper*, No. 2655, 1986, pp. 1-18.
[19] Bons, J.P., MacArthur, C.D., and Rivir, R.B., 1996, "The effect of high free-stream turbulence on film cooling effectiveness," *J. Turbomach*, v. 118, pp. 814-825.
[20] Kohli, A. and Bogard, D.G., 1998, "Effects of Very High Free-stream Turbulence on the Jet-Mainstream Interaction in a Film Cooling Flow," *J. Turbomach*, v. 120, pp. 785-790.
[21] Ames, F.E., 1998, "Aspects of Vane Film Cooling with High Turbulence: Part I - Heat Transfer," *J. Turbomach*, v. 120, pg. 768-776.
[22] Mayhew, J.E., Baughn, J.W., and Byerley, A.R., 2002, "The Effect of Free-stream Turbulence on Film Cooling Adiabatic Effectiveness", ASME Paper No. GT-2002-30172.
[23] Bunker, R.S., 2005, "A Review of Shaped Hole Turbine Film-Cooling Technology," *J. Heat Transfer*, v. 127, pp. 441-453.
[24] Thole K., Gritsch M., Schulz A., and Wittig, S., 1998, "Flowfield Measurements for Film-Cooling Holes with Expanded Exits *J. Turbomach.* v. 120, pp. 327-336.
[25] Haven, B.A., Yamagata, D.K., Kurosaka, M., Yamawaki, S., and Maya, T., "Anti-kidney pair of vortices in shaped holes and their influence on film cooling effectiveness," ASME Paper No. 97-GT-45
[26] Schroeder, R.P., and Thole, K.A., 2014, "Adiabatic Effectiveness Measurements for a Baseline Shaped Film Cooling Hole," ASME Paper No. GT2014-25992.
[27] Saumweber, C., Schulz, A., and Wittig, S., 2003, "Free-Stream Turbulence Effects on Film-Cooling with Shaped Holes", *J. Turbomach*, v. 125, pp. 65-73.
[28] Saumweber, C., and Schulz, A., 2012 "Free-Stream Effects on the Cooling Performance of Cylindrical and Fan-Shaped Cooling Holes", *J. Turbomach*, v. 134, pp. 1-12.
[29] Ames, F.E., Wang, C., and Barbot, P.A., 2003, "Measurement and prediction of the influence of catalytic and dry low NOx Combustor Turbulence on Vane Surface Heat Transfer," *J. Turbomach*, v. 125, pp. 210-220.
[30] Gandaparavu, P., and Ames, F.E., 2012 "The Influence of Leading Edge Diameter on Stagnation Region Heat Transfer Augmentation Including Effects of Turbulence Level, Scale, and Reynolds Number," *J. Turbomach*, v. 135, pp. 011008-1-8.
[31] Chowdhury, N.H.K. and Ames, F.E., 2013, "The response of high intensity turbulence in the presence of large stagnation regions," ASME Paper No. GT2013-95055.
[32] ANSYS FLUENT 6.3, 2006, FLUENT 6.3 User's Guide, Fluent, Inc., Lebanon, N.H.
[33] Spalart, P. and Allmaras, S., 1992, "A one-equation turbulence model for aerodynamic flows," Technical Report AIAA-92-0439, American Institute of Aeronautics and Astronautics.
[34] Moffat, R.J., 1988, "Describing the Uncertainties in Experimental Results", *Exp. Thermal & Fluid Science*, v. 1, pp. 3-17.
[35] Martini, P., and Schulz, A., 2004, "Experimental and Numerical Investigation of Trailing Edge Film Cooling by Circular Coolant Wall Jets Ejected From a Slot With Internal Rib Arrays," *J. Turbomach*, v. 126, pp. 229–236.

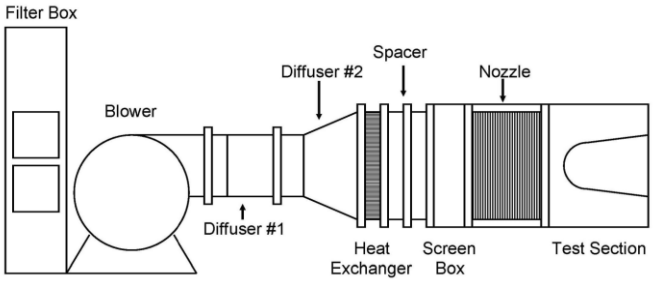


Figure 1.Schematic of UND's large scale cascade wind tunnel with cylindrical leading edge test section.

Table 1. Turbulence conditions for higher and lower Reynolds number conditions

| | $U_{ave}$ (m/s) | Tu | $L_x$ (cm) | Lu (cm) | ε ($m^2/s^3$) |
|---|---|---|---|---|---|
| AC | 9.11 | 0.130 | 3.52 | 6.36 | 42.1 |
| | 18.11 | 0.126 | 3.58 | 7.35 | 253.4 |
| ACS | 9.17 | 0.092 | 4.61 | 8.81 | 12.06 |
| | 17.6 | 0.090 | 4.44 | 9.49 | 68.63 |
| GR | 9.94 | 0.079 | 2.04 | 3.35 | 23.4 |
| | 18.95 | 0.081 | 2.35 | 3.53 | 163.4 |
| SG1 | 9.12 | 0.078 | 1.61 | 1.85 | 29.4 |
| | 17.87 | 0.079 | 1.12 | 1.97 | 216.0 |
| SG2 | 9.08 | 0.035 | 1.73 | 3.23 | 1.49 |
| | 17.61 | 0.035 | 2.13 | 2.85 | 12.1 |
| LT | 9.65 | 0.0076 | 5.02 | 154.5 | 0.0004 |
| | 18.71 | 0.0061 | 3.58 | 15.5 | 0.0144 |

Table 2. Table of boundary layer parameters taken in the discharge region of the shaped holes on the large leading edge test surface.

| File: | BAC1R3Y1 | BAC1R4Y3 | BACSR3Y1 | BACSR4Y1 |
|---|---|---|---|---|
| δ* (cm) | 0.0218 | 0.0174 | 0.0199 | 0.0154 |
| $\delta_2$ (cm) | 0.0101 | 0.0082 | 0.0090 | 0.0071 |
| H | 2.16 | 2.13 | 2.22 | 2.17 |
| Cf/2 | 0.0061 | 0.0040 | 0.0063 | 0.0041 |
| $Re_{\delta 2}$ | 54.0 | 94.5 | 51.6 | 85.6 |
| $U_\infty$ (m/s) | 8.63 | 19.34 | 9.28 | 19.66 |
| $Tu_0$ | 0.1371 | 0.1377 | 0.0933 | 0.0924 |
| $Lu_0$ (cm) | 6.17 | 7.08 | 9.48 | 9.81 |
| | | | | |
| File: | BGS2R3Y1 | BGS2R4Y5 | BLTR3Y1 | BLTR4Y5 |
| δ* (cm) | 0.0192 | 0.0158 | 0.0221 | 0.0163 |
| $\delta_2$ (cm) | 0.0086 | 0.0069 | 0.0098 | 0.0074 |
| H | 2.23 | 2.27 | 2.26 | 2.19 |
| Cf/2 | 0.0064 | 0.0038 | 0.0057 | 0.0036 |
| $Re_{\delta 2}$ | 50.2 | 85.6 | 60.1 | 95.0 |
| $U_\infty$ (m/s) | 9.43 | 20.42 | 9.99 | 21.10 |
| $Tu_0$ | 0.0350 | 0.0348 | 0.0076 | 0.0060 |
| $Lu_0$ (cm) | 3.23 | 2.85 | 154.5 | 15.5 |

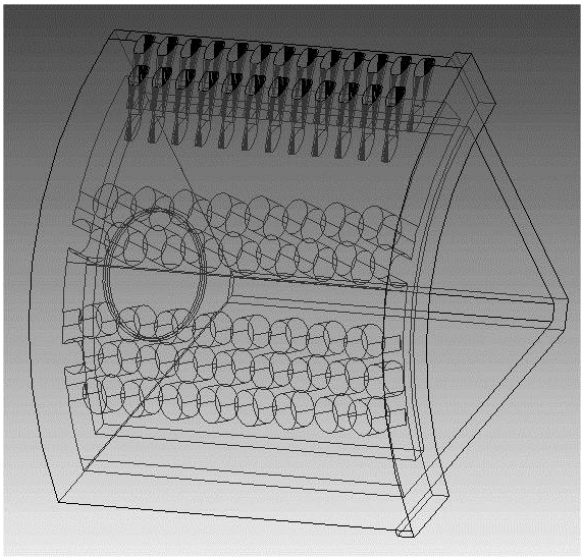

Figure 2. Schematic of shaped hole film cooling insert for large cylindrical leading edge test surface.

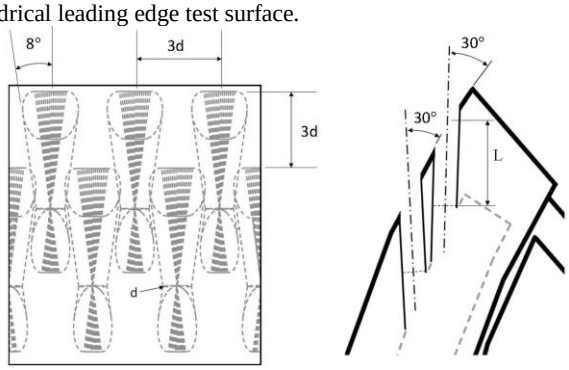


Figure 3. Schematic of shaped hole array and shaped holes as configured for the leading edge film cooling insert.

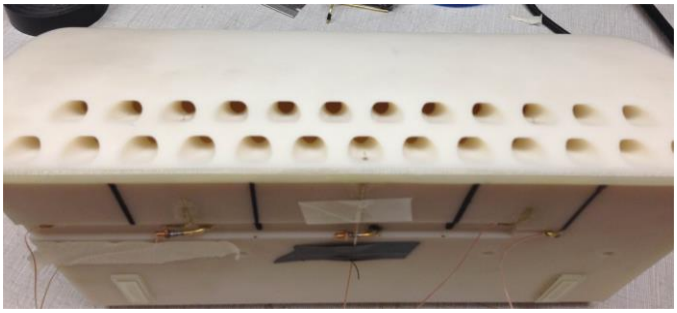

Figure 4. Photo of shaped hole insert showing full coverage staggered array with intra-hole thermocouples.

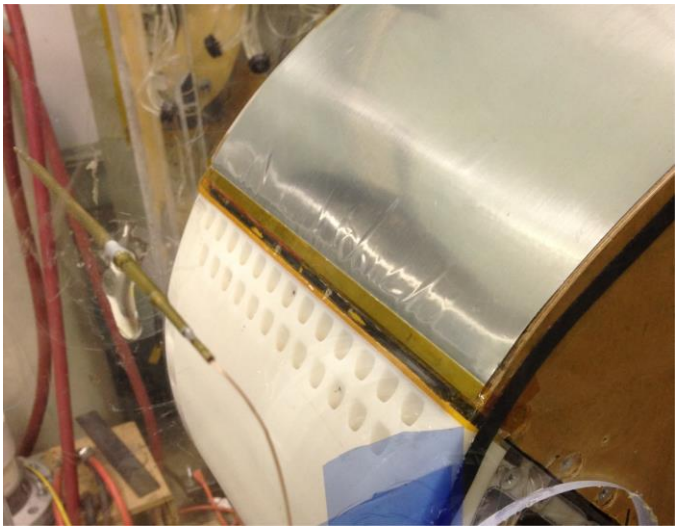

Figure 5. Photo of shaped hole insert installed onto cylinder upstream of bracket instrumentation and heat transfer foil.

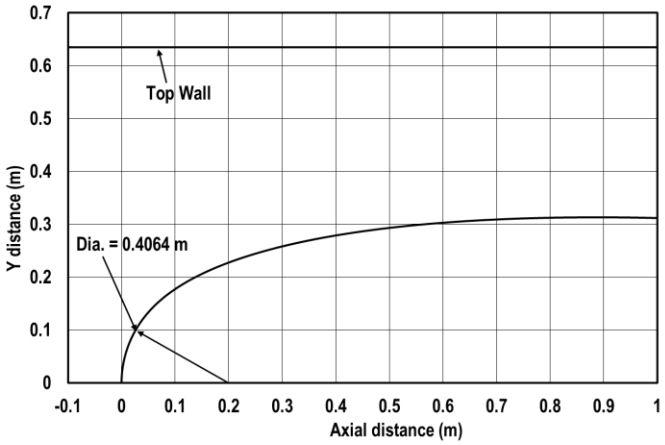


Figure 6. Schematic of large cylindrical leading edge test surface profile.

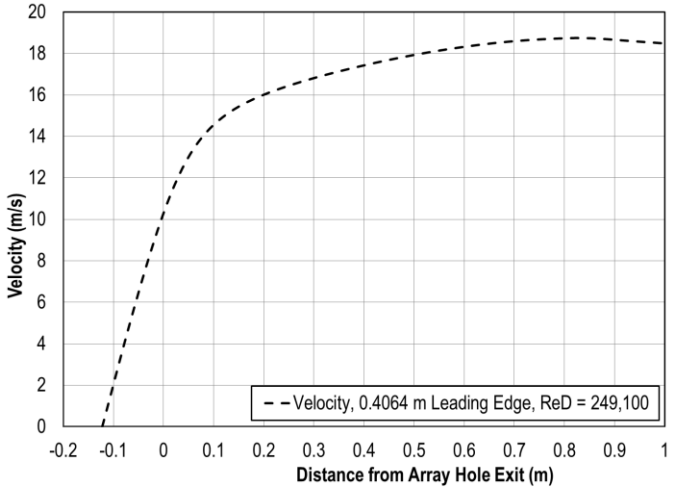


Figure 7. Predicted velocity distribution over larger cylindrical leading edge test surface.

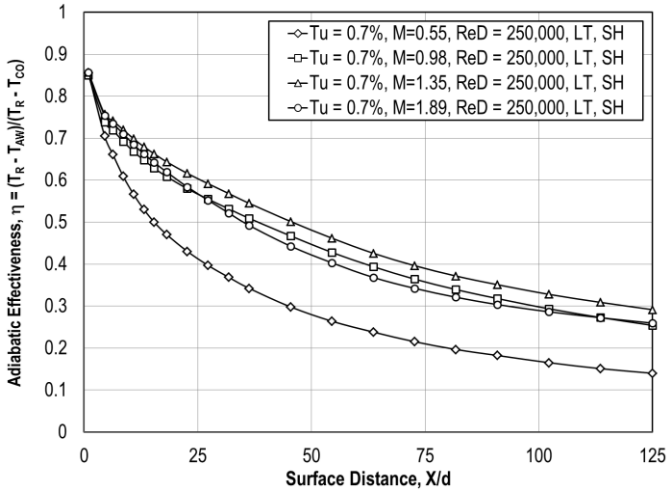


Figure 8. Adiabatic film cooling, low turbulence (LT), variable blowing ratios, larger diameter.

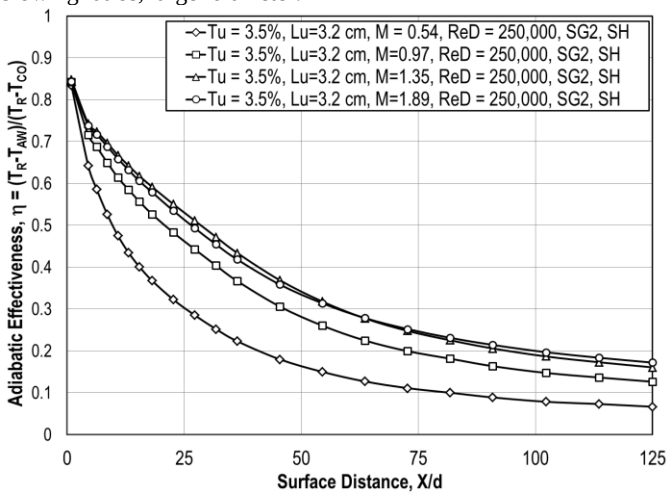


Figure 9. Adiabatic film cooling, small grid far turbulence (SG2), variable blowing ratios, larger diameter.

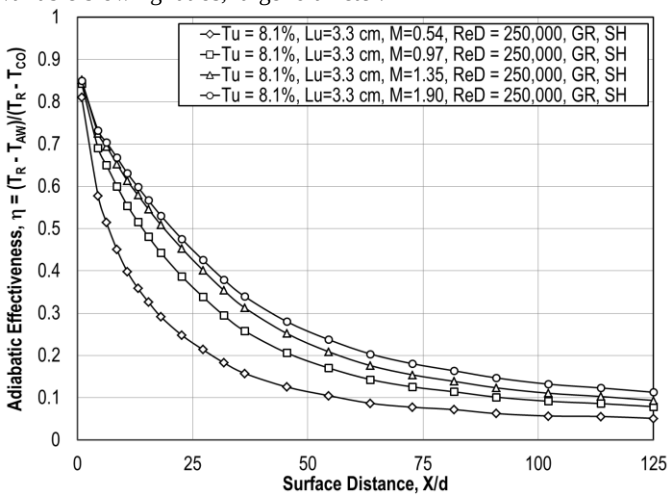


Figure 10. Adiabatic film cooling, grid turbulence (GR), variable blowing ratios, larger diameter.

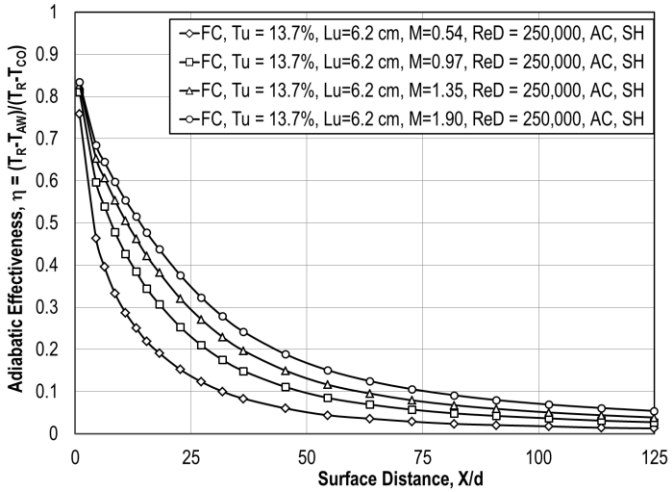


Figure 11. Adiabatic film cooling, aero-combustor turbulence (AC), variable blowing ratios, larger diameter.

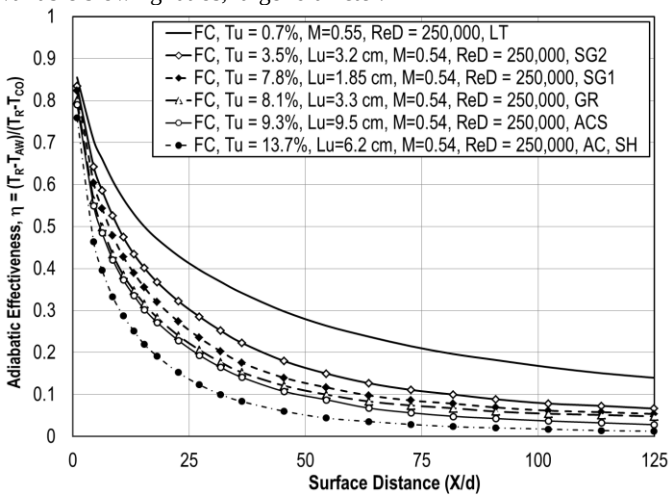


Figure 12. Adiabatic film cooling effectiveness, M = 0.54, variable turbulence condition, $Re_D$ = 250,000.

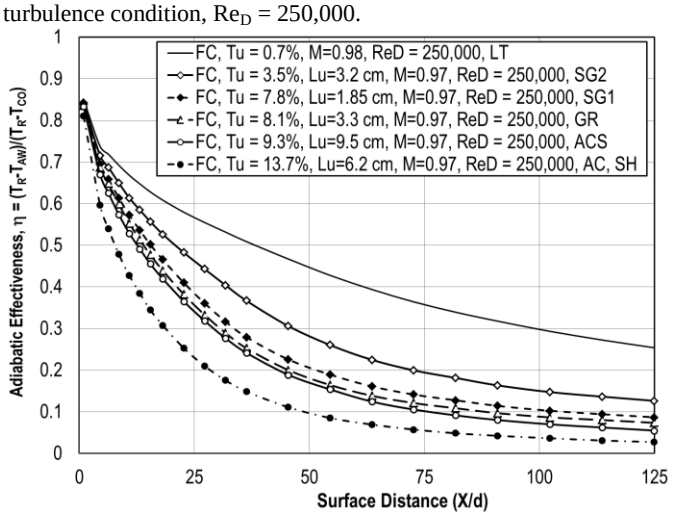


Figure 13. Adiabatic film cooling effectiveness, M = 0.97, variable turbulence conditions, $Re_D$ = 250,000.

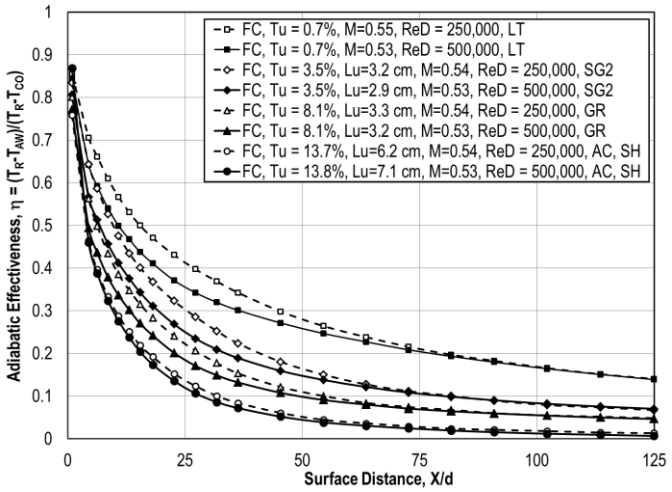


Figure 14. Adiabatic film cooling effectiveness, M = 0.54 comparing turbulence conditions and Reynolds numbers.

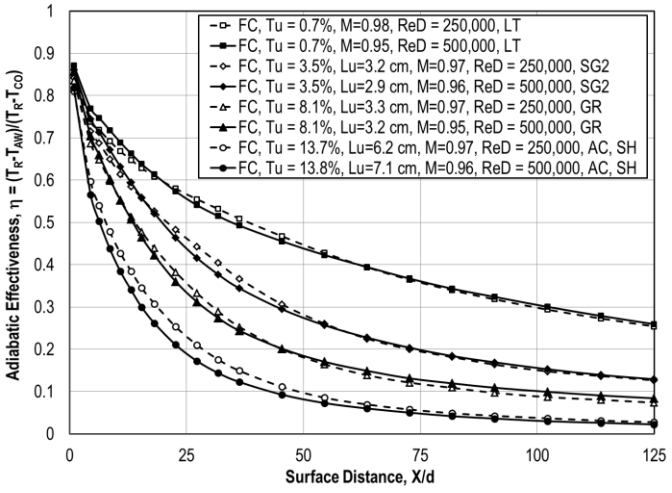


Figure 15. Adiabatic film cooling effectiveness, M = 0.96 comparing turbulence conditions and Reynolds numbers.

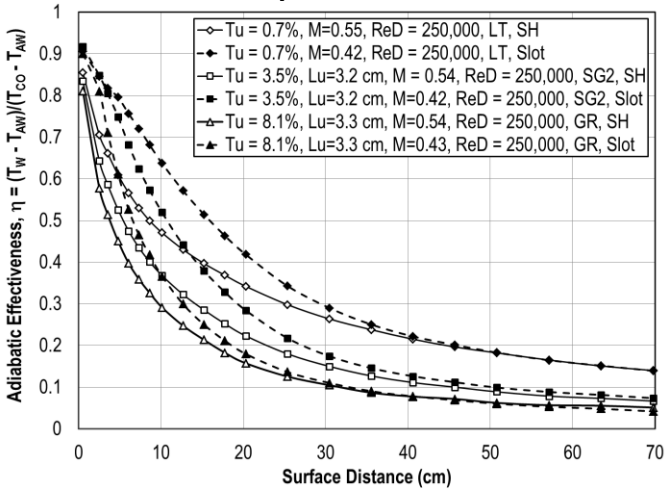


Figure 16. Adiabatic film cooling effectiveness, M = 0.54 comparing shaped holes and slot [2] at same mass flow rate, $Re_D$ = 250,000.

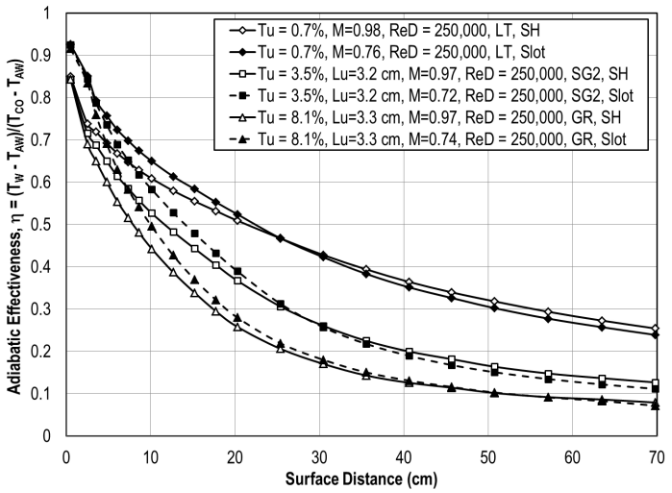


Figure 17. Adiabatic film cooling effectiveness, M = 0.95 comparing shaped holes and slot [2] at same mass flow rate, $Re_D$ = 250,000.

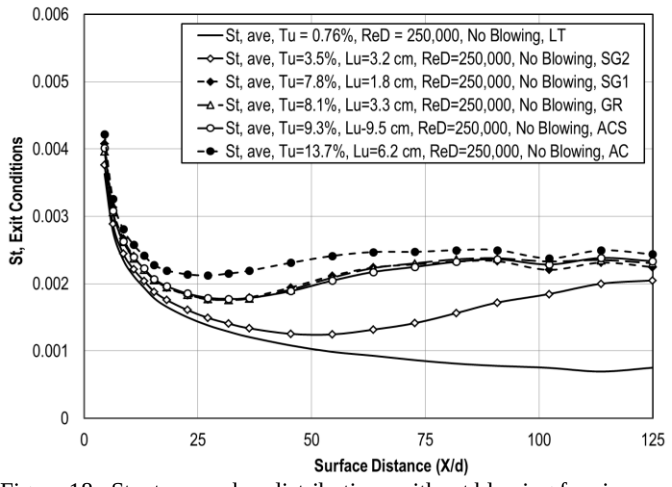


Figure 18. Stanton number distributions without blowing for six turbulence conditions, $Re_D$ = 250,000.

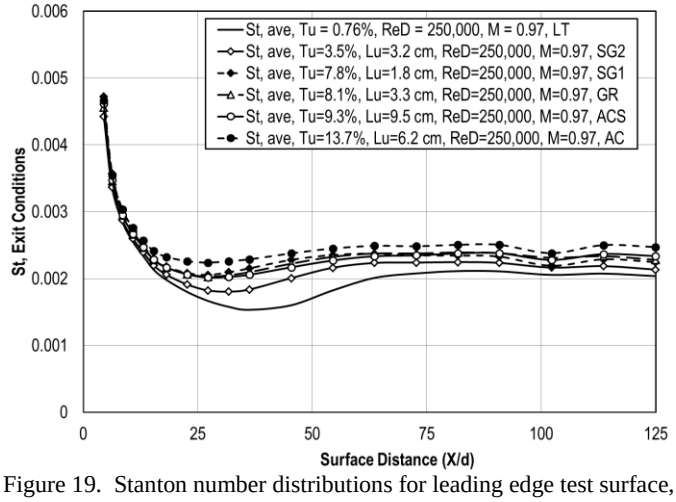


Figure 19. Stanton number distributions for leading edge test surface, M = 0.97, $Re_D$ = 250,000, for six turbulence conditions.

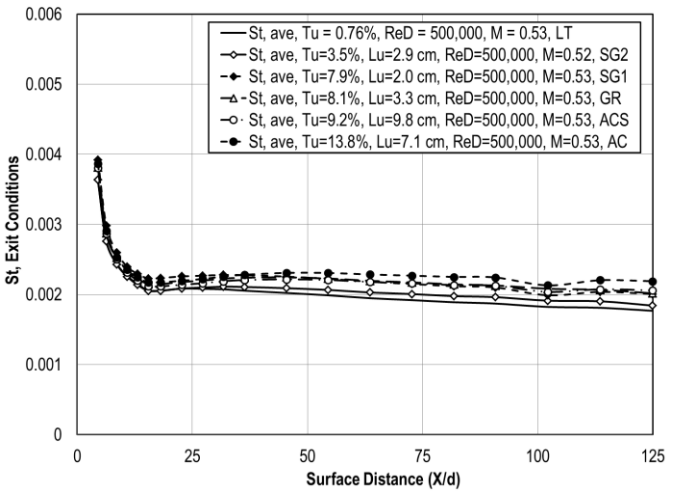


Figure 20. Stanton number distributions for leading edge test surface, M = 0.53, $Re_D$ = 500,000, for six turbulence conditions.

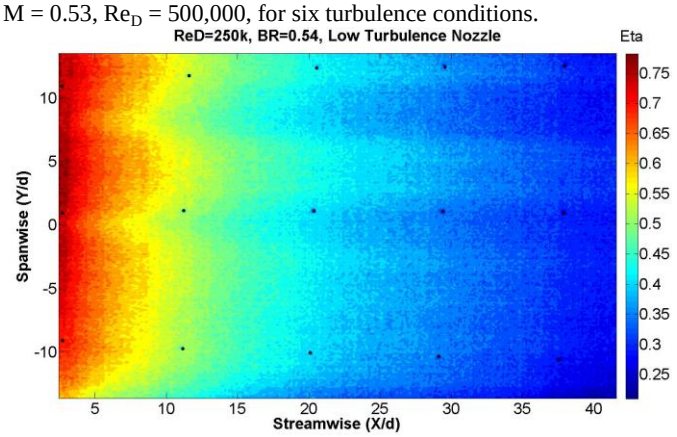


Figure 21. Full surface, IR, film cooling visualization, M = 0.54 low turbulence (LT) showing spanwise variation of film cooling effectiveness.

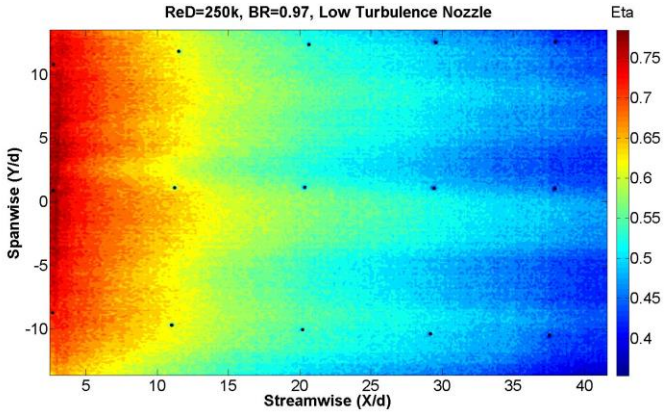


Figure 22. Full surface, IR, film cooling visualization, M = 0.97 low turbulence (LT) showing spanwise variation of film cooling effectiveness.

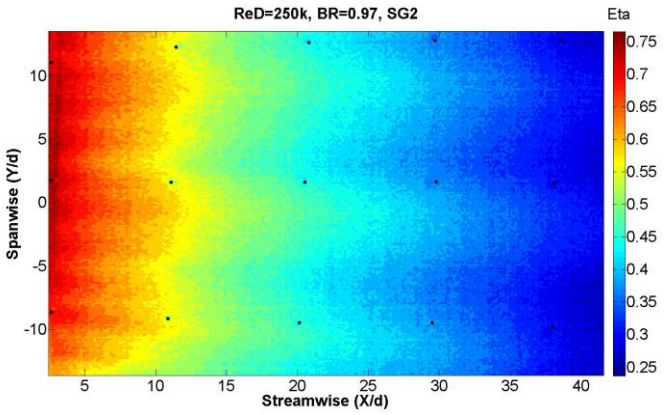


Figure 23. Full surface, IR, film cooling visualization, M = 0.97 small grid near (SG2) showing spanwise variation of film cooling effectiveness.

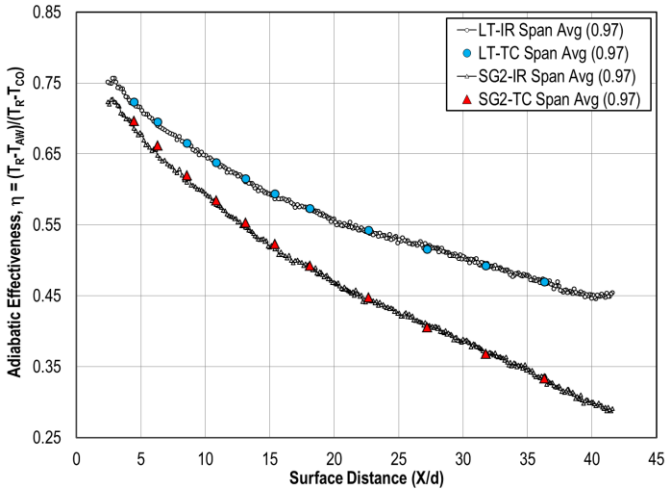


Figure 24. Adiabatic film cooling effectiveness, shaped holes, $Re_D$ = 250,000, comparing thermocouple data with span averaged full surface data.

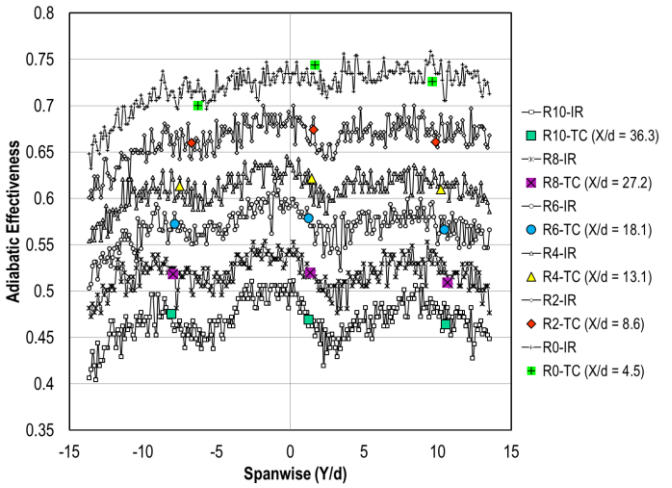


Figure 25. Comparison of IR camera data with thermocouple data at fixed X/d locations, low turbulence (LT), M = 0.95, $Re_D$ = 250,000.

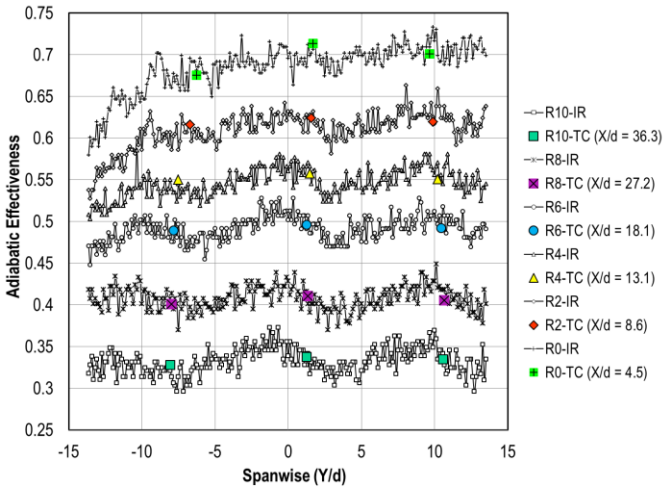


Figure 26, Comparison of IR camera data with thermocouple data at fixed X/d locations, small grid far (SG2), M = 0.97, $Re_D$ = 250,000.

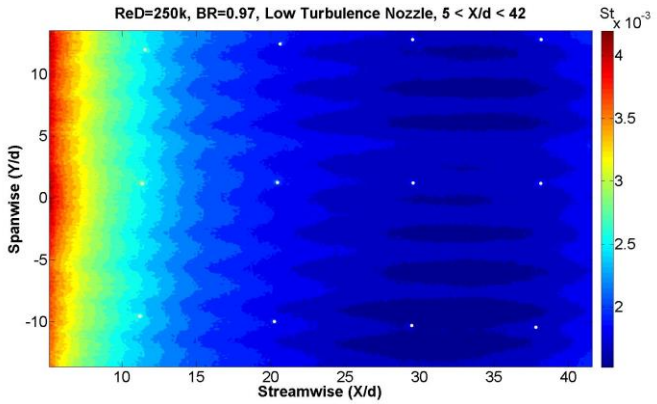


Figure 27. Full surface, IR, heat transfer visualization, M = 0.97 low turbulence (LT) showing spanwise variation of Stanton number, $Re_D$ = 250,000.